Materials Research Bulletin 112 (2019) 178–181

Contents lists available at ScienceDirect

Materials Research Bulletin

journal homepage: www.elsevier.com/locate/matresbu

Crystal structures and microwave dielectric properties of novel low-permittivity $Ba_{1-x}Sr_xZnSi_3O_8$ ceramics

Xiao-Qiang Song[a,b], Kang Du[a,b], Jie Li[a,b], Raz Muhammad[d], Wen-Zhong Lu[a,b], Xiao-Chuan Wang[a,b], Wen Lei[a,b,c,*]

[a] School of Optical and Electronic Information, Huazhong University of Science and Technology, Wuhan, 430074, PR China
[b] Key Lab of Functional Materials for Electronic Information (B), Ministry of Education, Wuhan, 430074, PR China
[c] Engineering Research Center for Functional Ceramics, Ministry of Education, Wuhan, 430074, PR China
[d] Department of Physics, Abdul Wali Khan University, Mardan, KP, Pakistan

ARTICLE INFO

Keywords:
Microwave dielectric properties
Zinc-feldspar
Low-relative permittivity

ABSTRACT

$Ba_{1-x}Sr_xZnSi_3O_8$ (x = 0.2–1.0) microwave dielectric ceramics were synthesized using the solid-state method at the temperature from 1087 °C to 1150 °C for 3 h. All compositions showed a single phase for $Ba_{1-x}Sr_xZnSi_3O_8$ when x increased from 0.2 to 1.0, and a phase transition from monoclinic to triclinic structure occurred between 0.8 and 1.0. The relative permittivity of $Ba_{1-x}Sr_xZnSi_3O_8$ ceramics decreased from 6.57 to 6.12 when the Ba^{2+} ions substituted by Sr^{2+} ions. However, the quality factor initially decreased from 34,735 GHz (x = 0.2) to 28,986 GHz (x = 0.4) and subsequently increased monotonously. The variation in the temperature coefficient of resonant frequency showed an opposite, slightly changing trend compared with that of the quality factor. A novel single-phase $SrZnSi_3O_8$, which possesses good microwave dielectric properties of ε_r = 6.12, $Q\times f$ = 78,064 GHz, and τ_f = −33.2 ppm/°C, was obtained for the first time at the sintering temperature of 1150 °C.

1. Introduction

With the expanding operating frequency ranges of microwave wireless communication, wireless communication is on the verge of entering its fifth generation. High frequency is required for ultrahigh-speed local area networks, electronic toll systems, and car anti-collision systems based on the intelligent transport systems [1,2]. Low-permittivity (ε_r < 15) microwave dielectric ceramics can be used as high-frequency substrates, dielectric antennae, high-accuracy capacitors, and millimeter-wave components, such as resonators and filters [3]. Thus, high-performance microwave dielectric ceramics with low permittivity is expected to attract considerable attention. For millimeter-wave wireless communication, microwave dielectric ceramics must present a low dielectric constant (ε_r) to reduce the transmission attenuation and the cross-coupling effect, a high-quality factor ($Q\times f$) to achieve excellent frequency selectivity, and a near-zero temperature coefficient of resonant frequency (τ_f) to ensure the stability of the transmitted frequency [4,5].

Silicates exhibit several interesting characteristics, such as ferroelectricity in Bi_2SiO_5 and $BaZnSiO_4$ [6,7], unique thermal expansion coefficient in $Ba_{1-x}Sr_xZn_2Si_2O_7$ [8], and microwave dielectric properties in $Mg_2Al_4Si_5O_{18}$ [9]. These interesting features are related to the materials' complex crystal structure consisting [SiO_4] tetrahedrons and other polyhedral. In general, silicates present a low permittivity value because of the Si–O bond in [SiO_4] tetrahedron, which contains 45% ionic bond and 55% covalent bond; the covalent bond reduces the relative permittivity because of the decrease of rattling effect [1]. In addition, numerous kinds of silicates, such as Zn_2SiO_4, $(Sr_{1-x}A_x)_2(Zn_{1-x}B_x)Si_2O_7$ (A = Ca, Ba and B = Co, Mg, Mn, Ni) and $CaAl_2Si_2O_8$ [10–12], have been explored. All of these silicates present a low permittivity value and a high quality factor, rendering the materials as good candidates for millimeter-wave devices.

In recent years, there have been several works focusing on feldspar-based microwave dielectric ceramics, which comprise plagioclase-feldspar-type and alkali-feldspar-type structures. The chemical formulas are $A[B_2C_2]O_8$ (A= Ca, Sr, Ba; B = Al, Ga; C = Si, Ge) and $A[BC_3]O_8$ (A = K, Na; B = Al, Ga; C = Si, Ge), respectively [12–16]. The feldspar crystal structure is composed of a three-dimensional framework of [Al/GaO_4] or [Si/GeO_4] tetrahedral. The charge balance due to the substitution of Al^{3+}/Ga^{3+} for Si^{4+}/Ge^{4+} is maintained by the addition of an interstitial alkali or alkali-earth ion [13]. Except for the most common feldspar, that is, zinc-feldspar, is rarely noticed. In 1970,

* Corresponding author at: School of Optical and Electronic Information, Huazhong University of Science and Technology, Wuhan, 430074, PR China.
E-mail address: wenlei@mail.hust.edu.cn (W. Lei).

https://doi.org/10.1016/j.materresbull.2018.12.026
Received 13 May 2018; Received in revised form 31 October 2018; Accepted 18 December 2018
Available online 19 December 2018
0025-5408/

Segnit et al. [17] synthesized the $BaZnSi_3O_8$ ceramics by the solid-state reaction method. Heuer et al. [18] reported the crystal structure of single-crystal $CaZnSi_3O_8$ prepared by hydrothermal method in 1998. Fehr et al. [19] called $CaZnSi_3O_8$ as zinc-feldspar and predicted the existence of $SrZnSi_3O_8$. In our previous work, $BaZnSi_3O_8$ ceramics was synthesized and its microwave dielectric properties were reported [3]. Thus so far, $SrZnSi_3O_8$ has not yet been synthesized, and its microwave dielectric properties have not been reported previously. In this work, Sr^{2+} ions were used as substitute for Ba^{2+} ions, and $Ba_{1-x}Sr_xZnSi_3O_8$ (x = 0.2-0.8) solid solution was prepared through the solid-state reaction method. Besides, the phase composition, microstructure, and microwave dielectric properties of $Ba_{1-x}Sr_xZnSi_3O_8$ (x = 0.2–1.0) ceramics were investigated.

2. Experimental procedure

The $Ba_{1-x}Sr_xZnSi_3O_8$ (x = 0.2–1.0) ceramics were prepared by conventional solid-state method using reagent grade $BaCO_3$ (99.8%), $SrCO_3$ (99.8%), ZnO (99.5%), SiO_2 (99.5%) powder as raw materials. According to desired stoichiometry, the raw materials were weighed to ball milled in a polyethylene jar for 12 h using ZrO_2 balls with deionized water. After drying at 85 °C, the mixtures were calcined in air at 1000 °C for 3 h with a heat rate of 5 °C/min. And then the powders were uniaxially pressed into samples with dimensions of 12 mm in diameter and approximately 6 mm in height under a pressure of 150 MPa. The samples were sintered in the temperature range of 1087 °C–1150 °C for 3 h at a heating rate of 5 °C/min, and then they were naturally cooled in the furnace after being cooled to 1000 °C at a rate of 1 °C/min.

The apparent density of the sintered samples was measured by Archimedes' method. The relative density ρ_{rel} was obtained by as formula follows [20]:

$$\rho_{rel} = \frac{\rho_{app}}{\rho_{the}} \tag{1}$$

where ρ_{app} and ρ_{the} were the apparent density and theoretical densities, respectively.

The X-ray diffraction (XRD) data were obtained using the XRD-7000 X-ray diffractometer (Shimadzu, Kyoto, Japan) with CuKα radiation. The microstructure and elemental mapping of the $Ba_{1-x}Sr_xZnSi_3O_8$ samples were observed by scanning electron microscope (Sirion 200, Netherlands) with an energy-dispersive X-ray spectrometer (JSM-6490LV, Japan). Grain size distributions were obtained using the Image J software. The values of ε_r and the unloaded $Q \times f$ value were measured within 12–14 GHz in the TE_{011} mode by Hakki and Coleman method [21] using a network analyzer (Agilent E8362B, Agilent Technologies, USA) and parallel silver boards. The τ_f value in the temperature range of 30–80 °C was calculated by Eq. (2):

$$\tau_f = \frac{1}{f(T_0)} \frac{[f(T_1) - f(T_0)]}{T_1 - T_0} \tag{2}$$

where $f(T_1)$ and $f(T_0)$ represented the resonant frequency at T_1 (80 °C) and T_0 (30 °C), respectively.

3. Results and discussion

Fig. 1 (a) shows the XRD patterns of $Ba_{1-x}Sr_xZnSi_3O_8$ (x = 0.2–1.0) ceramics sintered at their optimum temperature. The diffraction peaks that corresponded to $Ba_{1-x}Sr_xZnSi_3O_8$ (x = 0.2-0.8) are indexed to $BaZnSi_3O_8$ (PDF#23-0841), indicating that $Ba_{1-x}Sr_xZnSi_3O_8$ forms a solid solution with monoclinic structure (P21/m space group). However, for x = 1.0, $SrZnSi_3O_8$ is not assigned a PDF card. The lattice parameters of $BaZnSi_3O_8$ and $SrZnSi_3O_8$ were extracted from XRD data using the least-squares method. All the peaks are indexed accordingly, and the crystal structure information is given in the supplemental file.

Fig. 1 (b) presents the enlargement of the main diffraction peaks between 26.0° and 28.5°. Resulting from the substitution of Sr^{2+} ions for Ba^{2+} ions, the peaks shifts to high angles. This phenomenon is expected because the ionic radius of Sr^{2+} is 1.31 Å (CN = 9), which is smaller than that of Ba^{2+} ions (1.47 Å; CN = 9) [22]. Moreover, the two main diffraction peaks at approximately 26.5° approaches each other when x increases from 0.2 to 1.0. However, another diffraction peak appears on the left of the main diffraction peak when x = 1.0. This phenomenon is caused by the phase transition from the P21/m space group (x = 0.2-0.8) to the P-1 space group (x = 1.0), as verified from the indexed results in the supplemental file. Meanwhile, the intensity of the diffraction peaks gradually increase as x increased, corresponding to the increase in crystallinity in the matrix ceramics [9].

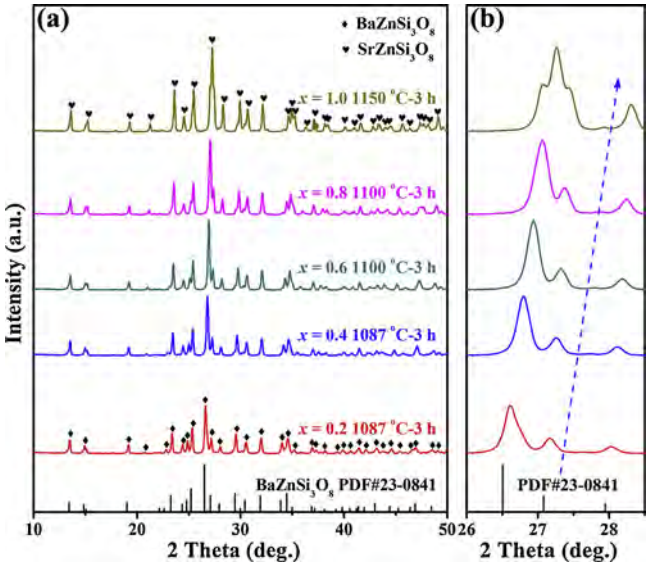

Fig. 1. (a) XRD powder diffraction patterns of $Ba_{1-x}Sr_xZnSi_3O_8$ (x = 0.2–1.0) ceramics sintered at 1087 °C–1150 °C for 3 h. (b) Enlargement of the main diffraction peaks between 26.0° and 28.5°.

Fig. 2 (a1)-(e1) present the microstructure of thermally etched $Ba_{1-x}Sr_xZnSi_3O_8$ (x = 0.2–1.0) ceramics sintered at 1087 °C to 1150 °C for 3 h. All of the compositions exhibit a dense microstructure, and small pores can be observed on the surface. Fig. 2 (a2)-(e2) and (a3)-(e3) show the backscattered electron (BSE) images and mapping of $Ba_{1-x}Sr_xZnSi_3O_8$ (x = 0.2–1.0) ceramics sintered at 1087 °C to 1150 °C for 3 h. No distinct grain can be observed (Fig. 2 (a2)-(e2)), and the elements of $Ba_{1-x}Sr_xZnSi_3O_8$ (x = 0.2–1.0) ceramics (Fig. 2 (a3)-(e3)) are evenly distributed on the surface, indicating that single-phase $Ba_{1-x}Sr_xZnSi_3O_8$ (x = 0.2–1.0) is formed. The average grain sizes estimated from Fig. 2 (a4)-(e4) are approximately 0.616, 0.723, 0.796, 0.874 and 1.098 μm, corresponding to x = 0.2-1.0. The increase in average grain size corresponds to the enhancement of the main diffraction peaks in Fig. 1, indicating an increasement in crystallinity [9].

Fig. 3 shows the apparent densities and relative densities of $Ba_{1-x}Sr_xZnSi_3O_8$ (x = 0.2–1.0) ceramics sintered at 1087 °C to 1150 °C for 3 h. The apparent densities of $Ba_{1-x}Sr_xZnSi_3O_8$ (x = 0.2–1.0) ceramics decreases monotonously from 3.55 g/cm^3 to 3.30 g/cm^3 because the atomic weight of Sr is smaller than that of Ba. The relative densities of all compositions are higher than 95%, and the effect of pores on the microwave dielectric properties is small [23].

Fig. 4 (a) shows the microwave dielectric properties of $Ba_{1-x}Sr_xZnSi_3O_8$ (x = 0.2–1.0) ceramics sintered at 1087 °C to 1150 °C for 3 h. The influence of porosity on ε_r is eliminated by the following equation [24]:

$$\varepsilon_{r-corr} = \varepsilon_r(1 + 1.5P) \tag{3}$$

where P is the porosity and can be calculated by the formula as follows:

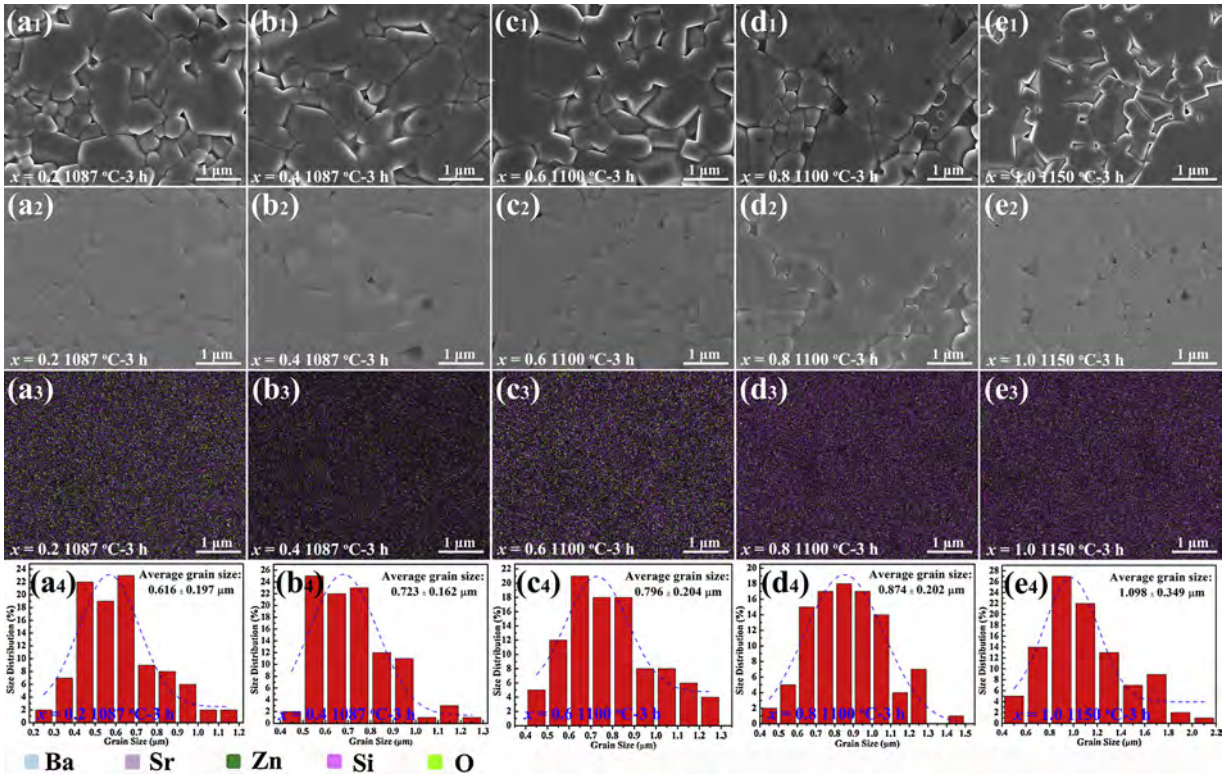

Fig. 2. (a1)-(e1) SEM images, (a2)-(e2) BSE images, (a3)-(e3) Mapping and (a4)-(e4) Grain size distribution of thermally etched $Ba_{1-x}Sr_xZnSi_3O_8$ (x = 0.2–1.0) ceramics sintered at 1087 °C–1150 °C for 3 h.

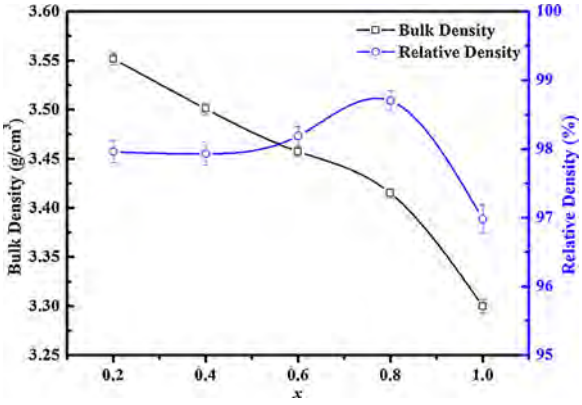

Fig. 3. Apparent densities and relative densities of $Ba_{1-x}Sr_xZnSi_3O_8$ (x = 0.2–1.0) ceramics sintered at 1087 °C–1150 °C for 3 h.

$$P = 1 - \rho_{rel} \quad (4)$$

The total ionic polarizability (α_D^T) of $Ba_{1-x}Sr_xZnSi_3O_8$ (x = 0.2–1.0) can be calculated by the additive rule [25,26]:

$$\alpha_D^T = (1-x)\alpha(Ba^{2+}) + x\alpha(Sr^{2+}) + \alpha(Zn^{2+}) + 3\alpha(Si^{4+}) + 8\alpha(O^{2-}) \quad (5)$$

where $\alpha(Ba^{2+})$, $\alpha(Sr^{2+})$, $\alpha(Zn^{2+})$, $\alpha(Si^{4+})$ and $\alpha(O^{2-})$ are the ionic polarizabilities of Ba^{2+}, Sr^{2+}, Zn^{2+}, Si^{4+}, and O^{2-}, respectively.

The relative permittivity (ε_r), porosity-corrected relative permittivity ($\varepsilon_{r\text{-corr}}$) and ionic polarizability (α_{theo}) of $Ba_{1-x}Sr_xZnSi_3O_8$ ceramics decreases monotonously when x increases from 0.2 to 1.0, thereby indicating that the ionic polarizability of $Ba_{1-x}Sr_xZnSi_3O_8$ plays a dominant role in controlling the relative permittivity [26,27]. The $Q\times f$ value initially decreases from 34,736 GHz for x = 0.2 to 28,986 GHz for x = 0.4, and subsequently increases to 78,064 GHz for x = 1.0 (Fig. 4 (b)). Variation of $Q\times f$ values of $Ba_{1-x}Sr_xZnSi_3O_8$ is similar to that of

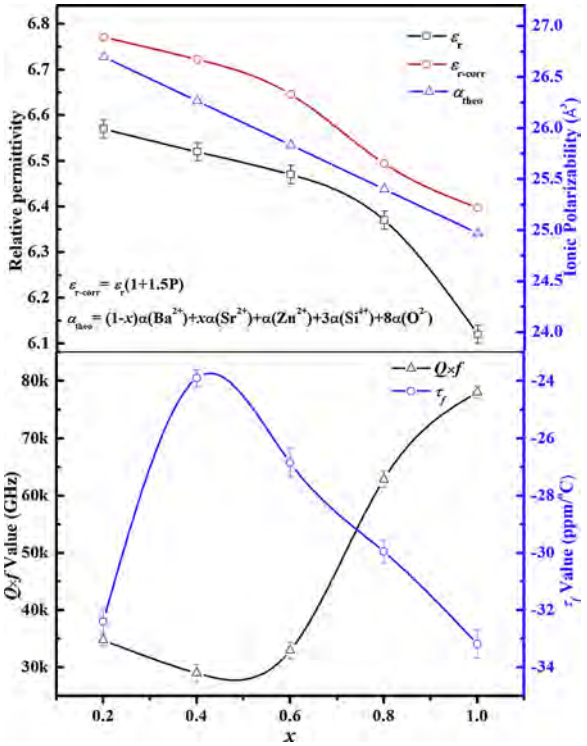

Fig. 4. (a) Relative permittivity (ε_r) and dielectric polarizability (α_{theo}) (b) $Q\times f$ value and τ_f value of $Ba_{1-x}Sr_xZnSi_3O_8$ (x = 0.2–1.0) ceramics sintered at 1087 °C–1150 °C for 3 h.

$(Sr_{1-x}A_x)_2ZnSi_2O_7$ (A = Ca, Ba) reported by M.T. Sebastian in 2010 [11]. They attributed this phenomenon to the difference in radius of the A-site cations, which leads to synergistic effects, such as the orderly

arrangement of the cations. $Ba_{1-x}Sr_xAl_2Si_2O_8$ and $Ba_{1-x}Ca_xAl_2Si_2O_8$ solid solutions belong to the typical feldspar-type crystal structure, which have a similar crystal structure to $Ba_{1-x}Sr_xZnSi_3O_8$. And the variation of $Q\times f$ for $Ba_{1-x}Sr_xAl_2Si_2O_8$, $Ba_{1-x}Ca_xAl_2Si_2O_8$ and $Ba_{1-x}Sr_xZnSi_3O_8$ solid solutions have the same trend [12,15]. Feldspar crystal structure is composed of a three-dimensional framework of $[Al/GaO_4]$ or $[Si/GeO_4]$ tetrahedral. It is easy to form a short-ordered arrangement Si and Al and long-ordered arrangement can be obtained after a long period of annealing. However, this Si:Al ordering cannot be detected by XRD due to the small difference in the X-ray scattering efficiencies of Al and Si. In $Ba_{1-x}Sr_xZnSi_3O_8$ solid solution, the three-dimensional framework is composed of $[ZnO_4]$ and $[SiO_4]$ tetrahedral. It is more likely to form a short-ordered arrangement between Zn^{2+} and Si^{4+} due to their large difference of ionic radius and valance state. Krzmanc attributes the variation of $Q\times f$ for $Ba_{1-x}Sr_xAl_2Si_2O_8$ and $Ba_{1-x}Ca_xAl_2Si_2O_8$ solid solutions to the change of cation ordering, which may also apply to $Ba_{1-x}Sr_xZnSi_3O_8$ solid solution. The variation trend of τ_f values and $Q\times f$ values is the opposite. The τ_f values vary slightly between -23.9 ppm/°C and -33.2 ppm/°C in the entire range of x. The most excellent microwave dielectric properties (namely, $\varepsilon_r = 6.12$, $Q\times f = 78{,}064$ GHz, and $\tau_f = -33.2$ ppm/°C) are obtained when $x = 1.0$ ($SrZnSi_3O_8$).

4. Conclusions

Low-permittivity $Ba_{1-x}Sr_xZnSi_3O_8$ ($x = 0.2$–1.0) low-permittivity microwave dielectric ceramics have been synthesized using the conventional solid-state method. XRD patterns, BSE images and mapping show that $Ba_{1-x}Sr_xZnSi_3O_8$ solid solutions with monoclinic structure (P21/m space group) are formed when x increases from 0.2 to 0.8. Importantly, a novel single-phase $SrZnSi_3O_8$ ceramic with triclinic structure (P-1 space group) is obtained for the first time. The relative permittivity of $Ba_{1-x}Sr_xZnSi_3O_8$ is dominated by ionic polarizability, and the ε_r decreases linearly from 6.57 to 6.12 when the Ba^{2+} ions are substituted by Sr^{2+} ions. However, the quality factor initially decreases from 34,735 GHz ($x = 0.2$) to 28,986 GHz ($x = 0.4$) and subsequently increases monotonously after a certain point. The τ_f values varies slightly between -23.9 ppm/°C and -33.2 ppm/°C in the total x range. The most excellent microwave dielectric properties (namely, $\varepsilon_r = 6.12$, $Q\times f = 78{,}064$ GHz, and $\tau_f = -33.2$ ppm/°C) are obtained when $x = 1.0$ ($SrZnSi_3O_8$).

Acknowledgements

This work was supported by the National Natural Science Foundation of China (NSFC-51572093, 51772107, and 61771215) and National Promotion Project of New Technology (JSCG2016110B006). The authors are grateful to the Analytical and Testing Center, Huazhong University of Science and Technology, for SEM analyses.

The authors are also grateful to Meng-Qi Xie for her help in English grammar modification.

References

[1] H. Ohsato, Microwave materials with high q and low dielectric constant for wireless communications, Mater. Res. Soc. Symp. Proc. 833 (2005) 55–62.
[2] X. Su, A. Wu, P.M. Vilarinho, Al_2TeO_6: Mechanism of phase formation and dielectric properties, Scripta Mater. 67 (2012) 927–930.
[3] X.Q. Song, W.Z. Lu, X.C. Wang, X.H. Wang, G.F. Fan, R. Muhammad, W. Lei, Sintering behaviour and microwave dielectric properties of $BaAl2\text{-}2_x(ZnSi)_xSi_2O_8$ ceramics, J. Eur. Ceram. Soc. 38 (2018) 1529–1534.
[4] H. Xiang, L. Fang, W. Fang, Y. Tang, C. Li, A novel low-firing microwave dielectric ceramic $Li_2ZnGe_3O_8$ with cubic spinel structure, J. Eur. Ceram. Soc. 37 (2017) 625–629.
[5] H. Zhou, X. Tan, J. Huang, N. Wang, G. Fan, X. Chen, Phase structure, sintering behavior and adjustable microwave dielectric properties of $Mg_{1-x}Li_{2x}Ti_xO_{1+2x}$ solid solution ceramics, J. Alloys. Compd. 696 (2017) 1255–1259.
[6] H. Taniguchi, A. Kuwabara, J. Kim, Y. Kim, H. Moriwake, S. Kim, T. Hoshiyama, T. Koyama, S. Mori, M. Takata, H. Hosono, Y. Inaguma, M. Itoh, Ferroelectricity driven by twisting of silicate tetrahedral chains, Angew. Chemie Int. Ed. English 52 (2013) 8088–8092.
[7] Z.Y. Zou, Z.H. Chen, X.K. Lan, W.Z. Lu, B. Ullah, X.H. Wang, Weak ferroelectricity and low-permittivity microwave dielectric properties of $Ba_2Zn_{(1+x)}Si_2O_{(7+x)}$ ceramics, J. Eur. Ceram. Soc. 37 (2017) 3065–3072.
[8] C. Thieme, H. Görls, C. Rüssel, $Ba_{1-x}Sr_xZn_2Si_2O_7$-A new family of materials with negative and very high thermal expansion, Sci. Rep. 5 (2015) 18040.
[9] K. Song, P. Liu, H. Lin, W. Su, J. Jiang, S. Wu, J. Wu, Z. Ying, H. Qin, Symmetry of hexagonal ring and microwave dielectric properties of $(Mg_{1-x}Ln_x)_2Al_4Si_5O_{18+x}$ (Ln = La, Sm) cordierite-type ceramics, J. Eur. Ceram. Soc. 36 (2016) 1167–1175.
[10] H.W. Chen, H. Su, H.W. Zhang, T.C. Zhou, B.W. Zhang, J.F. Zhang, X.L. Tang, Low-temperature sintering and microwave dielectric properties of $(Zn_{1-x}Co_x)_2SiO_4$ ceramics, Ceram. Int. 40 (2014) 14655–14659.
[11] T. Joseph, M.T. Sebastian, Microwave dielectric properties of $(Sr_{1-x}A_x)_2(Zn_{1-x}B_x)Si_2O_7$ ceramics (A = Ca, Ba and B = Co, Mg, Mn, Ni), J. Am. Ceram. Soc. 93 (2010) 147–154.
[12] M.M. Krzmanc, M. Valant, B. Jancar, D. Suvorov, Sub-solidus synthesis and microwave dielectric characterization of plagioclase feldspars, J. Am. Ceram. Soc. 88 (2005) 2472–2479.
[13] M.M. Krzmanc, M. Valant, D. Suvorov, A structural and dielectric characterization of $Na_xCa_{1-x}Al_{2-x}Si_{2+x}O_8$ (x = 0 and 1) ceramics, J. Eur. Ceram. Soc. 25 (2005) 2835–2838.
[14] M.M. Krzmanc, A. Meden, D. Suvorov, The correlation between the structure and the dielectric properties of $K_xBa_{1-x}Ga_{2-x}Ge_{2+x}O_8$ ceramics, J. Eur. Ceram. Soc. 27 (2007) 2957–2961.
[15] M.M. Krzmanc, M. Valant, D. Suvorov, The synthesis and microwave dielectric properties of $Sr_xBa_{1-x}Al_2Si_2O_8$ and $Ca_yBa_{1-y}Al_2Si_2O_8$ ceramics, J. Eur. Ceram. Soc. 27 (2007) 1181–1185.
[16] N. Qin, M.M. Krzmanc, A. Meden, D. Suvorov, Structural investigation of $K_xBa_{1-x}Ga_{2-x}Ge_{2+x}O_8$ solid solutions using the X-ray Rietveld method, J. Solid State Chem. 182 (2009) 1666.
[17] E.R. Segnit, A.E. Holland, The ternary system BaO-ZnO-SiO_2, Aust. J. Chem. 23 (1970) 1077–1085.
[18] M. Heuer, K. Bente, M. Steins, Crystal structure of calcium tectozincotrisilicate, $CaZnSi_3O_8$, Z. Krist-New. Cryst. St. 213 (1998) 691–692.
[19] K.T. Feh, A.L. Huber, Stability and phase relations of $Ca[ZnSi_3]O_8$, a new phase with feldspar structure in the system CaO-ZnO-SiO_2, Am. Mineral. 86 (2001) 21–28.
[20] S. Lei, H. Fan, X. Ren, J. Fang, L. Ma, H. Tian, Microstructure, phase evolution and interfacial effects in a new $Zn_{0.9}Mg_{0.1}TiO_3$-$ZnNb_2O_6$ ceramic system with greatly induced improvement in microwave dielectric properties, Scripta Mater. 146 (2018) 154–159.
[21] B.W. Hakki, P.D. Coleman, A dielectric resonant method of measuring inductive capacitance in the millimeter range, IRE Trans. Microwave Theory Technol. 8 (1960) 402–410.
[22] R.D. Shannon, Revised effective ionic radii and systematic studies of interatomie distances in halides and chaleogenides, Acta Crystallogr. A 32 (1976) 751–767.
[23] E.S. Kim, S.H. Kim, K.H. Yoon, Dependence of thermal stability on octahedral distortion of $(1\text{-}x)(Ca_{0.3}Li_{0.119}Sm_{0.427})TiO_3$-$xLnAlO_3$($Ln$ = Nd, Sm) ceramics, J. Ceram. Soc. Jpn. 112 (2004) S1645–S1649.
[24] S.D. Rama Rao, S. Roopas Kiran, V.R.K. Murthy, Correlation between structural characteristics and microwave dielectric properties of scheelite $Ca_{1-x}Cd_xMoO_4$ solid solution, J. Am. Ceram. Soc. 95 (2012) 3532-2537.
[25] (a) S. Lei, H. Fan, W. Chen, Z. Liu, M. Li, Structure, microwave dielectric properties, and novel low-temperature sintering of xSrTiO$_3$-(1-x) $LaAlO_3$ ceramics with LTCC application, J. Am. Ceram. Soc. 100 (2016) 235–246;
(b) R.D. Shannon, Dielectric polarizabilities of ions in oxides and fluorides, J. Appl. Phys. 73 (1993) 348–366.
[26] S.D. Ramarao, V.R.K. Murthy, Crystal structure refinement and microwave dielectric properties of new low dielectric loss AZrNb$_2$O$_8$ (A: Mn, Zn, Mg and Co) ceramics, Scripta Mater. 69 (2013) 274–277.